Meshing skin surfaces with certified topology

Kruithof, N.G.H.; Vegter, G.

Published in:
Meshing skin surfaces with certified topology

Meshing Skin Surfaces with Certified Topology

N.G.H. Kruithof* and G. Vegter
Department of Mathematics and Computing Science
University of Groningen,
P.O. Box 800, 9700 AV Groningen, The Netherlands
{nico,gert}@cs.rug.nl

Abstract

Skin surfaces are used for the modeling and visualization of molecules. They form a class of tangent continuous surfaces defined in terms of a set of balls (the atoms of the molecule) and a shrink factor. More recently, skin surfaces have been used to approximate arbitrary surfaces.

We present an algorithm that approximates a skin surface with a topologically correct mesh. The complexity of the mesh is linear in the size of the Delaunay triangulation of the balls, which is worst case optimal.

We also adapt two existing refinement algorithms to improve the quality of the mesh and show that the same algorithm can be used for meshing a union of balls.
Keywords: Skin Surfaces, Meshing, Isotopy, Delaunay triangulation.

1. Introduction

Skin surfaces, introduced by Edelsbrunner in [6], have a rich and simple combinatorial and geometric structure that makes them suitable for modeling large molecules in biological computing. Meshing such surfaces is often required for further processing of their geometry, like in numerical simulation and visualization. We present an algorithm for meshing skin surfaces with guaranteed topology.

Large molecules can be modeled using skin surfaces by representing each atom by a sphere. Atoms that lie close to each other are connected by smooth patches. A skin surface is parameterized by a set of weighted points (input balls) and a shrink factor. If the shrink factor is equal to one, the surface is just the boundary of the union of the input balls. If the shrink factor decreases, the skin surface becomes tangent continuous, due to the appearance of patches of spheres and hyperboloids connecting the shrunken balls.

*Partially supported by the IST Programme of the EU as a Shared-cost RTD (FET Open) Project under Contract No IST-006413 (ACS – Algorithms for Complex Shapes)

We present an algorithm in [12] that approximates an arbitrary smooth surface with a skin surface. The approximation is homeomorphic to the skin surface and the Hausdorff distance between the two surfaces is arbitrarily small.

Two surfaces embedded in three space are isotopic if there is a continuous deformation in the ambient space that transforms one surface into the other one. In particular, isotopic surfaces are homeomorphic. The algorithm presented in this paper constructs a mesh isotopic to the skin surface in two steps: it constructs a coarse, isotopic mesh which is subsequently improved. For the second step a broad range of refinement algorithms can be used. We implemented the refinement algorithms of Chew [5] and Kobbelt [10]. The $\sqrt{3}$-subdivision algorithm by Kobbelt is very fast, and refines the size of the triangles. However, it does not improve the quality of the mesh elements in terms of angle size. Chew's algorithm improves the quality of the mesh in terms of the angles and size of the triangles. The quality mesh is suitable for numerical computations. Our version of these algorithms preserve the isotopy property.

For a shrink factor one, the skin surface of a set of balls is the union of these balls. Hence, the algorithm can also be used to mesh the union of a set of balls.

Related work. Most existing meshing algorithms for implicit surfaces do not guarantee topological equivalence of the surface and the mesh constructed. Examples are the marching cubes algorithm [13] and the marching triangulation method [9] Our paper [11] presents a marching triangulation method for meshing skin surfaces by carefully choosing the step size during the walk over the mesh. However, as the shrink factor goes to one or to zero, the size of the mesh goes to infinity.

General isotopic meshers are proposed in [2, 14]. However the number of critial points (proportional to the number of balls) makes them not suitable.

The algorithms in [3, 8] construct a topologically correct mesh approximating a skin surface in the special case of a shrink factor 0.5. It is likely that this algorithm can be generalized to work for arbitrary shrink factors, but this would

Ninth International Conference on Computer Aided Design and Computer Graphics (CAD/CG 2005)
0-7695-2473-7/05 $20.00 © 2005 IEEE

probably result in a denser mesh in order to guarantee the topology. The algorithm is also rather slow. Another approach is found in [4]. We could not verify the claim that the mesh produced by the algorithm in this paper is homeomorphic to the skin surface.

Contribution. The main contribution compared to [3] is that our approach works for any shrink factor. We also establish isotopy, which is stronger than topological equivalence and our algorithm is much faster. It constructs a mesh in minutes where the algorithm presented in [3] takes hours. It is more flexible in the sense that we generate a coarse mesh that is isotopic to the skin surface and then refine it by different algorithms, whereas the algorithm in [3] immediately constructs a homeomorphic quality mesh.

On the theoretical side, we analyze the structure of the mixed complex and decompose the mixed cells into tetrahedra. Within a tetrahedron the intersection with the skin surface is either empty or a topological disk. It is then fairly easy to extract an isotopic mesh.

Outline. In Section 2 we extend the theory of skin surfaces as presented in [6]. We start by introducing a hierarchical combinatorial structure on the mixed complex. Section 3 describes the construction of the coarse mesh and establishes the isotopy between this mesh and the skin surface. Section 3.1 describes two methods to improve the coarse mesh. Finally, we describe our implementation and give results in Section 4 and 4.

2. Definitions

This section first briefly reviews skin surfaces introduced in [6] and then introduces some new concepts specific to the meshing algorithm.

Skin surfaces. A skin surface is defined in terms of a finite set of weighted points $\mathcal{P}$ and a shrink factor s, with $0 \leq s \leq 1$. A weighted point $\hat{p} = (p, \mathrm{P}) \in \mathbb{R}^d \times \mathbb{R}$ corresponds to a ball with center p and radius $\sqrt{\mathrm{P}}$. A pseudo-distance between two weighted points is given by: $\pi(\hat{p}, \hat{q}) = \|p - q\|^2 - \mathrm{P} - \mathrm{Q}$, where $\hat{p} = (p, \mathrm{P})$, $\hat{q} = (q, \mathrm{Q})$ and $\|\cdot\|$ denotes the Euclidean distance. The pseudo-distance $\pi(\hat{p}, x)$ of a weighted point $\hat{p}$ to an (unweighted) point x is the pseudo-distance of $\hat{p}$ to the weighted point centered at x with zero weight.

The space of weighted points inherits a vector space structure from $\mathbb{R}^{d+1}$ via the bijective map $\Pi : \mathbb{R}^d \times \mathbb{R} \to \mathbb{R}^{d+1}$, defined by $\Pi(\hat{p}) = (x_1, \ldots, x_d, \|p\|^2 - \mathrm{P})$, with $p = (x_1, \ldots, x_d)$. Addition of two weighted points and the multiplication of a weighted point by a scalar are defined in the vector space structure inherited under Π.

Starting from a weighted point $\hat{p} = (p, \mathrm{P})$, the shrunken weighted point $\hat{p}^s$ is defined as $\hat{p}^s = (p, s \cdot \mathrm{P})$. The set $\mathcal{P}^s$ is the set obtained by shrinking every weighted point of $\mathcal{P}$ by a factor s.

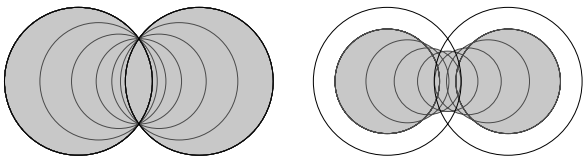

Figure 1. Construction of the skin curve of two weighted points (the two dashed circles) for a shrink factor $s = 1$ and $s = 0.5$.

The skin surface $\mathtt{skn}^s\mathcal{P}$ and its body $\mathtt{bdy}^s\mathcal{P}$ associated with a set of weighted points $\mathcal{P}$, are defined by

$$\mathtt{bdy}^s\mathcal{P} = \cup(\mathtt{conv}\ \mathcal{P})^s \quad (1)$$

$$\mathtt{skn}^s\mathcal{P} = \partial\ \mathtt{bdy}^s\mathcal{P}. \quad (2)$$

Here $\mathtt{conv}\ (\mathcal{P}) \subset \mathbb{R}^d \times \mathbb{R}$ is the convex hull – with respect to the vector space structure inherited under Π – of a set of weighted points $\mathcal{P}$, whereas ∂ denotes the boundary – in $\mathbb{R}^d$ – of the union of the corresponding set of set of balls. For circles defined by the vector space Π and shrunk with the shrink factor s, see Figure 1. The boundary of these circles is the skin curve.

Delaunay triangulation. The Delaunay triangulation and Voronoi diagram are used to decompose the skin surface into patches of spheres and hyperboloids. We briefly give the definition of these structures and mention some properties.

The (weighted) Voronoi diagram (or: the power diagram) $\mathrm{Vor}(\mathcal{P})$ of a set of weighted points $\mathcal{P}$ is the subdivision of $\mathbb{R}^d$ into cells $\nu_{\mathcal{X}}$ that have smaller power distance to the weighted points in $\mathcal{X} \subseteq \mathcal{P}$ than to any other weighted point in $\mathcal{P}$: $\nu_{\mathcal{X}} = \bigcap_{\hat{p} \in \mathcal{X}, \hat{p}' \in \mathcal{P}} \{x \in \mathbb{R}^d | \pi(\hat{p}, x) \leq \pi(\hat{p}', x)\}$.

The dual of the Voronoi diagram is the Delaunay triangulation (or: regular triangulation) $\mathrm{Del}(\mathcal{P})$. We denote a Delaunay simplex of a set $\mathcal{X} \subseteq \mathcal{P}$, with $\nu_{\mathcal{X}} \neq \emptyset$, by $\delta_{\mathcal{X}}$. Recall that $\delta_{\mathcal{X}} = \mathtt{conv}\ (\{p | \hat{p} \in \mathcal{X}\})$.

Since the affine hulls of $\delta_{\mathcal{X}}$ and $\nu_{\mathcal{X}}$ are complementary and orthogonal, they always intersect in a single point, the *center* $c(\mathcal{X})$ of $\mathcal{X}$.

General position. In the remainder of this paper we assume general position, by which we mean that no $d + 2$ weighted points are equidistant to a point in $\mathbb{R}^d$ and no $k+2$ centers of weighted points lie on a common k-flat for $k = 0, \ldots, d-1$. Several methods like [7] exist to symbolically perturb a data set and ensure these conditions.

The mixed complex. The mixed complex $\mathrm{Mix}^s(\mathcal{P})$, associated with a scalar $s \in [0, 1]$, is an intermediate complex between the Delaunay triangulation and the Voronoi diagram. Each mixed cell in the mixed complex is obtained

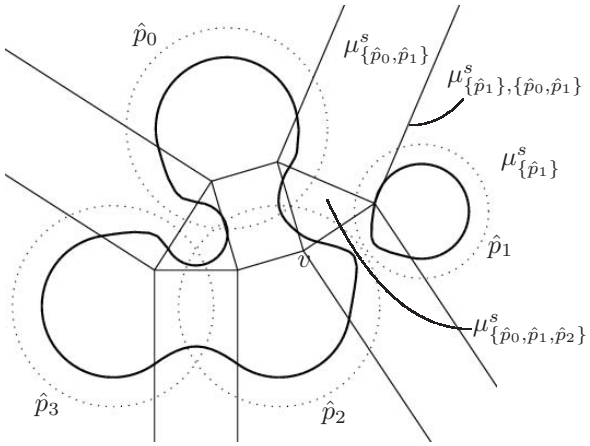

Figure 2. The skin curve of four weighted points (the dotted circles). Each mixed cell contains parts of an hyperbola or a circle. Some labels of mixed cells are given. Note that $v = \mu^s_{\{\hat{p}_0,\hat{p}_2\},\{\hat{p}_1,\hat{p}_2\}} = \mu^s_{\{\hat{p}_2\},\{\hat{p}_0,\hat{p}_1,\hat{p}_2\}}$.

by taking Minkowski sums of shrunken Delaunay simplices and their dual Voronoi cells.

Definition 1. *For* $\delta_{\mathcal{X}} \in \mathrm{Del}(\mathcal{P})$ *the* mixed cell $\mu^s_{\mathcal{X}}$ *is defined by* $\mu^s_{\mathcal{X}} = (1-s)\cdot\delta_{\mathcal{X}} \oplus s\cdot\nu_{\mathcal{X}}$.

Here $\cdot$ denotes the multiplication of a set by a scalar and $\oplus$ denotes the Minkowski sum. For $s = 0$ the mixed cell is the Delaunay cell. When s increases it deforms affinely into the Voronoi cell for $s = 1$. A mixed ℓ-cell is constructed from a Delaunay ℓ-simplex.

Within a mixed ℓ-cell $\mu^s_{\mathcal{X}}$, the skin surface is a quadratic surface (sphere or hyperboloid) of the form $I^{-1}_{\mathcal{X}}(0)$, with:

$$I_{\mathcal{X}}(x) = -\frac{1}{1-s}\sum_{i=1}^{\ell} x_i^2 + \frac{1}{s}\sum_{i=\ell+1}^{3} x_i^2 - R^2, \qquad (3)$$

and $x = (x_1, x_2, x_3)$. More precisely, $\mathtt{skn}^s\mathcal{X} \cap \mu^s_{\mathcal{X}} = I^{-1}_{\mathcal{X}}(0) \cap \mu^s_{\mathcal{X}}$. The coordinate system is orthonormal with its origin at the center of $\mathcal{X}$, and such that the first ℓ coordinates span the affine hull of $\delta_{\mathcal{X}}$, see [6].

In the plane, the intersection of a skin curve with a mixed cell is either part of a circle or hyperbola, cf. Figure 2.

The following observation holds trivially for mixed cells of type 0 and 3. For mixed cells of type 1 and 2 it follows from the choice of the coordinate axis and the construction of the mixed cells.

Observation 2. *Each proper face of a mixed cell* $\mu^s_{\mathcal{X}}$ *is perpendicular to a symmetry set of* $I_{\mathcal{X}}$

Since the symmetry axis and the symmetry plane of the hyperboloid are perpendicular, each face of a mixed cell of type 1 or 2 is parallel to the other symmetry set.

Polyhedral complex. The mixed complex is a polyhedral complex. The 3-cells of this polyhedral complex are formed by the mixed cells. We give a more detailed description of its structure.

Definition 3. *For* $\mathcal{X}, \mathcal{X}' \in \mathcal{P}$*, with* $\nu_{\mathcal{X}}, \nu_{\mathcal{X}'} \neq \emptyset$*, a polyhedral cell* $\mu^s_{\mathcal{X},\mathcal{X}'}$ *is defined as* $\mu^s_{\mathcal{X},\mathcal{X}'} = \mu^s_{\mathcal{X}} \cap \mu^s_{\mathcal{X}'}$.

It is clear that a polyhedral cell $\mu^s_{\mathcal{X},\mathcal{X}'}$ is non-empty, for $0 < s < 1$, if the Delaunay and Voronoi cells of $\mathcal{X}$ and $\mathcal{X}'$ have a non-empty intersection. Or, equivalently, if $\nu_{\mathcal{X}\cap\mathcal{X}'}, \nu_{\mathcal{X}\cup\mathcal{X}'} \in \mathrm{Vor}(\mathcal{P})$. For nonempty polyhedral cells, the following lemma describes the structure of the mixed complex.

Lemma 4. *A mixed cell* $\mu^s_{\mathcal{X},\mathcal{X}'}$ *is not empty iff* $\nu_{\mathcal{X}\cap\mathcal{X}'}$ *and* $\nu_{\mathcal{X}\cup\mathcal{X}'}$ *are nonempty.*

In that case, $\mu^s_{\mathcal{X},\mathcal{X}'} = (1-s)\cdot\delta_{\mathcal{X}\cap\mathcal{X}'} \oplus s\cdot\nu_{\mathcal{X}\cup\mathcal{X}'}$.

Proof omitted in this version

The anchor point. For the construction of the coarse mesh in Section 3, we define a tetrahedral complex that decomposes the skin surface into topological disks. We use anchor points as vertices of this tetrahedral complex.

Definition 5. *Let* A *be a convex set and* p *a point in* $\mathbb{R}^3$*. Then the* anchor point $a_p(A)$ *is the point in* A *closest to* p*.*

We are interested in the case where A is a polyhedral cell $\mu^s_{\mathcal{X},\mathcal{X}'}$, and p the center $c(\mathcal{X})$.

On $\mu^s_{\mathcal{X},\mathcal{X}'}$, $I_{\mathcal{X}}$ has two types of critical points: interior and boundary critical points. All critical points are anchor points of a face of the mixed cell, viz. Figure 3. However, not all anchor points are critical points, e.g. the point that is both the anchor point of a vertex and an edge in Figure 3(a).

Lemma 6. *A (boundary or regular) critical point of* $I_{\mathcal{X}}$ *on a polyhedral cell* $\mu^s_{\mathcal{X},\mathcal{X}'}$ *is the anchor point of* $\mu^s_{\mathcal{X},\mathcal{X}'}$ *or the anchor point of one of its faces with respect to* $c(\mathcal{X})$.

Proof. The center $c(\mathcal{X})$ is the only critical point of the quadratic function $I_{\mathcal{X}}$. If $c(\mathcal{X})$ is contained in $\mu^s_{\mathcal{X},\mathcal{X}'}$, then it is the anchor point $a_{c(\mathcal{X})}(\mu^s_{\mathcal{X},\mathcal{X}'})$.

It remains to show that all boundary critical points are also anchor points. By Observation 2, a face of $\mu^s_{\mathcal{X},\mathcal{X}'}$ is either parallel or perpendicular to the symmetry sets of $I_{\mathcal{X}}$. Hence, if $c(\mathcal{X})$ projects onto the facet, then the facet has a boundary critical point. By definition, this point is the anchor point of the facet with respect to $c(\mathcal{X})$. □

3. The meshing algorithm

This section describes the construction of a tetrahedral complex for which the intersection of a cell with the skin surface is either empty or a topological disk and constructs the coarse mesh.

Monotonicity condition. For now, we only give the main condition imposed on the tetrahedral complex. First, we require that each tetrahedron is contained in a single mixed

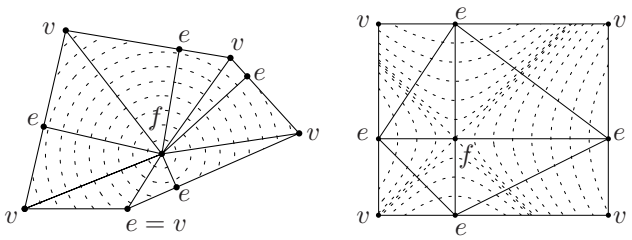

(a) Circular facets (b) Hyperbolic facets

Figure 3. The anchor points of two-dimensional polyhedral cells. Each anchor point is labeled by the type its cell (f for face, e for edge and v for vertex). The triangulation constructed in Section 3.1 is also shown.

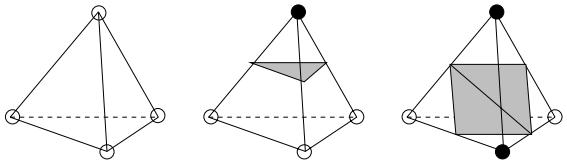

Figure 4. The three different configurations of a tetrahedron. White and black vertices lie on different sides of the skin surface.

cell. Recall that the skin surface restricted to a mixed cell $\mu^s_{\mathcal{X}}$ is a subset of the quadric $I_{\mathcal{X}}^{-1}(0)$, cf. Equation (3). Express a point $x = (x_1, x_2, x_3)$ in the local coordinate system of $I_{\mathcal{X}}$.

Condition 7 (Monotonicity). *Let ab be a line segment contained in a mixed cell $\mu^s_{\mathcal{X}}$ of type ℓ, with $I_{\mathcal{X}}(a) \leq I_{\mathcal{X}}(b)$. The segment ab satisfies the monotonicity condition if $x_1^2 + \ldots + x_\ell^2$ is non-increasing and $x_{\ell+1}^2 + \ldots + x_3^2$ is non-decreasing on the segment from a to b.*

Note that $x_1^2 + \ldots + x_\ell^2$ and $x_{\ell+1}^2 + \ldots + x_3^2$ are the distances to the two symmetry sets. Hence a segment has the monotonicity condition when the distance to the symmetry sets is monotone and they are not both increasing or decreasing. From Equation (3) we conclude:

Observation 8. *If line segment ab satisfies the monotonicity condition, then $I_{\mathcal{X}}$ is monotonically increasing on ab.*

If all edges satisfy the monotonicity condition, then a generalized monotonicity condition holds for all cells.

Lemma 9. *Let $\mu^s_{\mathcal{X}}$ be a mixed cell of type ℓ and let $v_1, \ldots, v_n$ be the vertices of a cell of the tetrahedral complex in $\mu^s_{\mathcal{X}}$, with $I_{\mathcal{X}}(v_i) \leq I_{\mathcal{X}}(v_j)$ if $i < j$.*

If the monotonicity condition holds for all edges then, each segment ab, with $a \in \texttt{conv}\,(v_1, \ldots, v_k)$ and $b \in \texttt{conv}\,(v_{k+1}, \ldots, v_n)$, for $k \in \{1, \ldots, n\}$, satisfies the monotonicity condition.

The lemma follows from the fact that $x_1^2 + \ldots + x_\ell^2$ is non-increasing and $x_{\ell+1}^2 + \ldots + x_3^2$ is non-decreasing on the piecewise linear curve connecting $v_1, \ldots, v_n$.

Mesh extraction. The coarse mesh is extracted from the tetrahedral complex by the marching tetrahedra algorithm [15]. Each edge of the tetrahedral complex intersects the skin surface at most once by Observation 8. We mesh the skin surface in a tetrahedron based on the number of vertices inside the skin surface as depicted in Figure 4.

Theorem 10. *A tetrahedral complex for which each edge satisfies the monotonicity condition has two properties:*

1. *each cell intersects the skin surface in a topological disk and*
2. *the mesh extracted from the tetrahedral complex is isotopic to the skin surface.*

Proof. Let V^- and V^+ be the vertices of a k-cell of the tetrahedral complex inside and outside the skin surface, respectively. Consider the set of line segments ab with $a \in \texttt{conv}\,(V^-)$, $b \in \texttt{conv}\,(V^+)$. The set of line segments is empty if the cell does not intersect the skin surface. If the cell intersects the skin surface, then the set of line segments spans the cell and the line segments may intersect but only at their endpoints. On faces of the cell, the line segments are defined consistently because then the construction is based on the labels of vertices of the face.

By Lemma 9, each segment satisfies the monotonicity condition. Hence $I_{\mathcal{X}}$ is monotone on ab. Since a lies inside and b outside the skin surface, ab intersects the skin surface in a single point. Because the segments span the tetrahedron, the skin surface within the cell is a topological disk.

Each segment also intersects the coarse mesh transversally in a single point. The isotopy is constructed by parameterizing the mesh and the skin surface with these segments and using linear interpolation between the parameterizations. □

3.1. The tetrahedral complex

In this section we construct the tetrahedral complex. First, we triangulate the facets and then the polyhedral cells.

All vertices of the tetrahedral complex are anchor points of polyhedral cells. An anchor point on the boundary of its polyhedral cell coincides with another anchor point. In that case we collapse the vertex. For simplicity, we assume that the anchor point lies in the interior of the mixed cell.

Subdividing facets of polyhedral cells. Based on the shape of the contour lines of $I_{\mathcal{X}}$, we distinguish two types of facets: *circular* and *hyperbolic* facets. Since the skin surface is tangent continuous, a facet obtains the same type from both incident cells. Examples of the triangulation of these facets are given in Figure 3.

0-7695-2473-7/05 $20.00 © 2005 IEEE

Circular facets are triangulated by adding an edge from the anchor point of the facet to each anchor point on the boundary of the facet, i.e., either the anchor point of an edge or a vertex. Since the anchor point of the facet is the point closest to the center of the sphere, the distance to the center increases monotonically on each edge and each edge satisfies the monotonicity condition.

Hyperbolic facets are rectangles with edges parallel or perpendicular to the symmetry axis of the corresponding hyperboloid, cf. Observation 2. We first triangulate the face similar to the circular facets and then flip the edges between the anchor points of the face and a vertex.

Subdividing polyhedral cells of type 0 and 3. These mixed cells contain spheres. By definition, the anchor point of the cell is the point closest to the center. Hence, each line segment from the anchor point of the mixed cell to another point in the mixed cell satisfies the monotonicity condition. We already constructed the triangulation of the boundary of the mixed cell and triangulate the entire cell by adding edges from the anchor point of the cell to each vertex on the boundary. The tetrahedra are formed by taking the join of the anchor point of the mixed cell and a triangle on the the triangulated boundary of the mixed cell.

Subdividing polyhedral cells of type 1 and 2. The mixed cell contains a hyperboloid patch of the skin surface and the mixed cell is a prism with its base parallel to the symmetry plane of the hyperboloid. The hyperbolic facets of the prism are the facets that are parallel to the symmetry axis. We split the prism in the plane parallel to the symmetry plane and through the anchor point of the mixed cell.

Consider the base of the split prism furthest away from the symmetry plane. Its anchor point is the point with maximal distance to the symmetry plane and minimal distance to the symmetry axis. Therefore, all line segments starting in this anchor point satisfy the monotonicity condition. We triangulate the split mixed cell by adding edges from the anchor point of the base to all vertices on the boundary. The tetrahedra are the join of a triangle on the triangulated boundary and the anchor point of the base.

Complexity analysis. In many real world applications is the size of the Delaunay triangulation linear in the number of input balls. However, the worst case complexity is quadratic. The size of the mixed complex is linear in the size of the Delaunay triangulation. The number of tetrahedra within a mixed cell is linear in the complexity of the mixed cell and within each tetrahedron we construct at most two triangles.

Lemma 11. *The size of the coarse mesh is linear in the size of the Delaunay triangulation.*

Mesh enhancement. The topologically correct mesh obtained with the marching tetrahedra algorithm is rather coarse and may contain long and skinny triangles. We used two existing methods to enhance this mesh. The *sqrt-3 subdivision method* [10] splits each triangle into 9 sub-triangles and then moves the newly created vertices towards the skin surface along the transversal segments. The refinement by *Chew's algorithm* [5] constructs a triangulation for which the triangles have angles between 30 and 120 degrees. During the refinement, we test whether the isotopy is maintained. Before we apply Chew's algorithm we remove small edges. This reduces the size of the final mesh considerably.

Molecule	Our algorithm			Dynamic	Marching
	Coarse	Sqrt-3	Chew		
pdb7tmn	1s	2s	5s	10m00s	5s
DNA	14s	29s	55s	35m12s	51s
Gramacidin A	8s	31s	1m13s	1h35m23s	3m22s

Table 1. Performance comparison

4. Implementation

We implemented the meshing and refinement algorithms described above in C++ using CGAL [1]. First we compute the Delaunay triangulation of the weighted points. From this triangulation we extract the mixed complex and triangulate it, as described in Section 3.

Examples and experiments. We compare our algorithm with the results in [4]. Those tests are run on a Pentium 4 running at 2.54GHZ. To test our algorithm we used an AMD Athlon 1800+ which is a little slower. We tested our algorithm on various molecules, computing only the coarse mesh, the coarse mesh and one additional $\sqrt{3}$-subdivision step and the coarse mesh and Chew's algorithm. For timings see Table 1. Note that both our algorithm and the marching algorithm [4] are significantly faster than the dynamic skin algorithm [3]. However, we believe that [4] does not come with topological guarantees.

Figure 6 shows the molecule pdb7tmn. In Figure 6(d) we enlarged a part of the coarse mesh and applied the Sqrt-3 method in Figure 6(e). Note that the triangles remain skinny. Figure 6(f) shows the result of applying Chew's algorithm directly to the coarse mesh. Because of small edges in the coarse mesh, there are also small edges in parts with low curvature. When we remove small edges, viz. Figure 6(g), before we apply Chew's algorithm, we obtain Figure 6(h).

5. Conclusion and future work

We presented an algorithm that constructs a mesh that is isotopic to the skin surface and discuss two methods to refine this mesh. The algorithm we present is static in the sense that it generates a mesh for a fixed set of input balls. The rigid foundation of the tetrahedral complex makes us

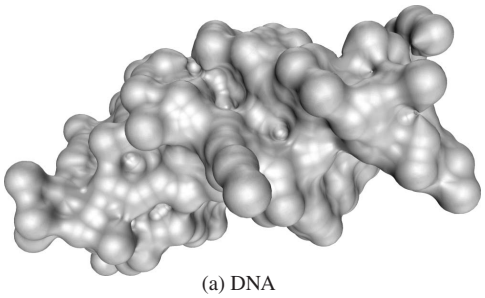

(a) DNA

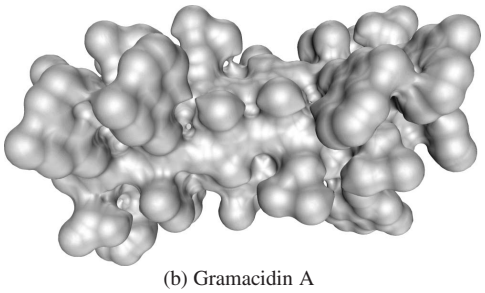

(b) Gramacidin A

Figure 5. Two larger molecules.

believe that it is also possible to maintain the coarse mesh while deforming the input set. This is important for deforming molecules.

References

[1] Computational Geometry Algorithms Library. `http://www.cgal.org`.

[2] J.-D. Boissonnat, D. Cohen-Steiner, and G. Vegter. Isotopic implicit surface meshing. In *STOC*, pages 301–309, 2004.

[3] H-L. Cheng, T.K. Dey, H. Edelsbrunner, and J. Sullivan. Dynamic skin triangulation. *Discrete Comput. Geom.*, 25:525–568, 2001.

[4] H.-L. Cheng and X.-W. Shi. Guaranteed quality triangulation of molecular skin surfaces. In *IEEE Visualization*, 2004.

[5] L. Chew. Guaranteed quality Delaunay meshing in 3d. In *Proc. 13th Annu. ACM Sympos. Comput. Geom.*, pages 391–393, 1997.

[6] H. Edelsbrunner. Deformable smooth surface design. *Discrete Comput. Geom.*, 21:87–115, 1999.

[7] H. Edelsbrunner and E. P. Mücke. Simulation of simplicity: A technique to cope with degenerate cases in geometric algorithms. *ACM Trans. Graph.*, 9(1):66–104, 1990.

[8] H. Edelsbrunner and A. Üngör. Relaxed scheduling in dynamic skin triangulation. In *Japanese Conf. Comput. Geom.*, pages 135–151, 2002.

[9] Erich Hartmann. A marching method for the triangulation of surfaces. *The Visual Computer*, 14(3):95–108, 1998.

[10] Leif Kobbelt. $\sqrt{3}$-subdivision. In *Proc. 27th ann. conf. on Comp. graphics and interactive techniques*, pages 103–112. ACM Press/Addison-Wesley Publishing Co., 2000.

[11] N.G.H. Kruithof and G. Vegter. Triangulating skin surfaces. Technical report, Rijksuniversiteit Groningen, 2003.

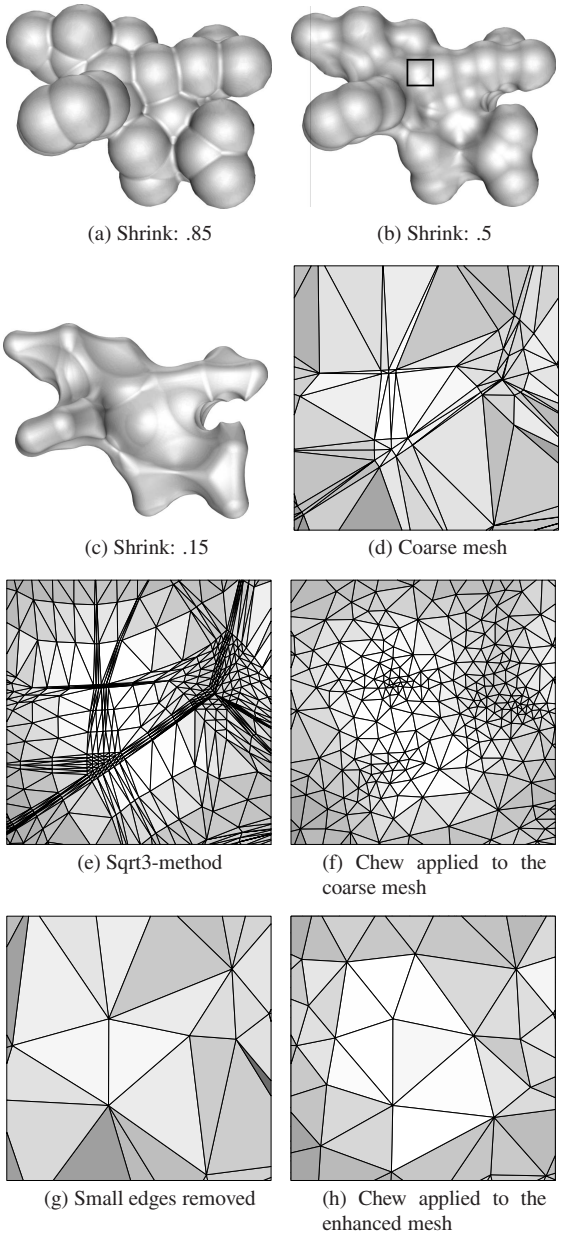

(a) Shrink: .85

(b) Shrink: .5

(c) Shrink: .15

(d) Coarse mesh

(e) Sqrt3-method

(f) Chew applied to the coarse mesh

(g) Small edges removed

(h) Chew applied to the enhanced mesh

Figure 6. pdb7tmn.

[12] Nico Kruithof and Gert Vegter. Approximation by skin surfaces. *Computer-Aided Design*, 36:1075–1088, 2004.

[13] W. Lorensen and H. Cline. Marching cubes: a high resolution 3d surface construction algorithm. *Comput. Graph.*, 21(4):163–170, 1987.

[14] B.T. Stander and J.C. Hart. Guaranteeing the topology of an implicit surface polygonization for interactive modeling. In *SIGGRAPH '97*, pages 279–286, 1997.

[15] G.M. Treece, R.W. Prager, and A.H. Gee. Regularised marching tetrahedra: improved iso-surface extraction. *Computers and Graphics*, 23(4):583–598, 1999.

0-7695-2473-7/05 $20.00 © 2005 **IEEE**